Can blue-green infrastructure mitigate waterborne infection risks through recreational activities in densely urbanized waterways?

This supplementary material provides background information to Petrucci and Derx et al.: "Can blue-green infrastructure mitigate waterborne infection risks through recreational activities in densely urbanized waterways? " The supplementary material is structured as follows:

S1: Climate scenarios summarizes the climate scenarios used in the study

S2: PCSWMM model set up describes the configuration and calibration of the PCSWMM model for the urban drainage catchment.

S3: Bioretention modelling details the setup of bioretention cells in PCSWMM, using literature-based design parameters

S4: Water quality data presents the observed microbial background concentrations in river water (Enterococci, *Cryptosporidium*, *Giardia*) and the fitted statistical distributions used in the model.

S5: Rainfall-runoff model (HBV) summarizes the hydrological model structure based on the HBV framework

S6: Additional results - Hydrological model result present the simulated frequency of combined sewer overflow (CSO) events under different climate scenarios (63, 73, 77) and the three planning horizons (C20, NTF, LTF) and all the varying levels of BGI implementation (0% to 50% with 5% interval), including the effects of additional storage.

S7: Additional results - Microorganisms' concentration in the river present simulated seasonal mean concentrations of *Enterococci*, *Cryptosporidium*, and *Giardia* under different climate scenarios (63, 73, 77) for the three planning horizons (C20, NTF, LTF) and BGI implementation levels (0% to 50% with 5% interval).

S8: Additional results – Time series presents *Giardia* infection risk and CSO flow for a representative July month under the C73 climate scenario for each planning horizon (C20, NTF, LTF).

S9: Sensitivity analysis presents a linear sensitivity analysis assessing the influence of background river concentrations (C_0) and CSO-related concentrations on infection risk for *Giardia* and *Cryptosporidium*.

S1 : Climate scenarios

C63: pr_SDM_CNRM-CERFACS-CNRM-CM5_rcp45_r1i1p1_SMHI-RCA4

C73: ICHEC-EC-EARTH_rcp85_r1i1p1_KNMI-RACMO22E

C77: IPSL-IPSL-CM5A-MR_rcp85_r1i1p1_IPSL-INERIS-WRF331F

Table. S1-1. Climate scenario

	Climate scenario	
1 (C63)	**pr_SDM_CNRM-CERFACS-CNRM-CM5_rcp45_r1i1p1_SMHI-RCA4**	Scenario with moderate mitigation efforts
2 (C73)	**ICHEC-EC-EARTH_rcp85_r1i1p1_KNMI-RACMO22E**	Business-as-usual scenario (high emission)
3 (C77)	**IPSL-IPSL-CM5A-MR_rcp85_r1i1p1_IPSL-INERIS-WRF331F**	Business-as-usual scenario (high emission)
4	pr_SDM_CNRM-CERFACS-CNRM-CM5_rcp45_r1i1p1_CLMcom-CCLM4-8-17	Used in Derx et al. (2023)
5	pr_SDM_CNRM-CERFACS-CNRM-CM5_rcp45_r1i1p1_CNRM-ALADIN53	
6	pr_SDM_CNRM-CERFACS-CNRM-CM5_rcp85_r1i1p1_CLMcom-CCLM4-8-17	
7	pr_SDM_CNRM-CERFACS-CNRM-CM5_rcp85_r1i1p1_CNRM-ALADIN53	
8	pr_SDM_CNRM-CERFACS-CNRM-CM5_rcp85_r1i1p1_SMHI-RCA4	
9	pr_SDM_ICHEC-EC-EARTH_rcp45_r1i1p1_KNMI-RACMO22E	
10	pr_SDM_ICHEC-EC-EARTH_rcp45_r3i1p1_DMI-HIRHAM5	
11	pr_SDM_ICHEC-EC-EARTH_rcp45_r12i1p1_SMHI-RCA4	
12	ICHEC-EC-EARTH_rcp85_r12i1p1_CLMcom-CCLM4-8-17	
13	ICHEC-EC-EARTH_rcp85_r12i1p1_SMHI-RCA4	
14	ICHEC-EC-EARTH_rcp85_r3i1p1_DMI-HIRHAM5	
15	IPSL-IPSL-CM5A-MR_rcp45_r1i1p1_IPSL-INERIS-WRF331F	
16	IPSL-IPSL-CM5A-MR_rcp45_r1i1p1_SMHI-RCA4	
17	IPSL-IPSL-CM5A-MR_rcp85_r1i1p1_SMHI-RCA4	
18	SDM_MPI-M-MPI-ESM-LR_rcp45_r1i1p1_CLMcom-CCLM4-8-17	
19	SDM_MPI-M-MPI-ESM-LR_rcp45_r1i1p1_SMHI-RCA4	
20	SDM_MPI-M-MPI-ESM-LR_rcp85_r1i1p1_CLMcom-CCLM4-8-17	
21	SDM_MPI-M-MPI-ESM-LR_rcp85_r1i1p1_SMHI-RCA4	
22	pr_SDM_ICHEC-EC-EARTH_rcp45_r12i1p1_CLMcom-CCLM4-8-17	Inconsistencies in the time series
23	MOHC-HadGEM2-ES_rcp45_r1i1p1_SMHI-RCA4	Inconsistencies in the time series
24	MOHC-HadGEM2-ES_rcp45_r1i1p1_CLMcom-CCLM4-8-17	Underestimations of rainfall
25	MOHC-HadGEM2-ES_rcp85_r1i1p1_CLMcom-CCLM4-8-17	Underestimations of rainfall
26	MOHC-HadGEM2-ES_rcp85_r1i1p1_SMHI-RCA4	Inconsistencies in the time series

Table S1.1 shows the studied climate scenarios. The fist 21 climate scenarios (bold black and grey) were used in Derx et al. (2023), the red scenario were rejected either due to inconsistencies in the time series or underestimations of rainfall. The first three (bold black) were used in the present paper because they are representative of the climate variability.

S2 : PCSWMM model set up

Table. S2-1. Parameters values for the urban drainage catchment in the PCSWMM model before adding BGI

Name	Area (ha)	Width (m)	Flow Length (m)	Imperv. (%)	Slope (%)
SC10	30	500	600	92	4.1
SC20	30	500	600	92	4.1
SC30	120	1800	666.7	92	4.1
SC40	120	1800	666.7	65	4.1
SC50	16.5	400	412.5	92	4.1
SC60	105	1600	656.3	92	4.1
SC70	45	1000	450	92	4.1
SC80	45	1000	450	65	4
SC90	180	1650	1090.9	100	4
SC100	180	2500	720	92	5.1
SC110	60	1200	500	90	5.1
SC120	50	1100	454.5	90	5
SC130	90	1650	545.4	65	1.4
SC140	150	2500	600	95	7.3
SC150	240	2500	960	65	7.3
SC160	225	3000	750	65	1.4
SC170	165	2250	733.3	90	3.1
SC180	240	3000	800	90	4
SC190	37.5	750	500	100	4
SC200	165	1650	1000	100	2.4
SC210	90	1650	545.5	65	3.9
SC220	90	1650	545.5	65	4

Table. S2-2. Concentration of the microorganism in the dry weather

Microorganisms	DWF concentration
Cryptosporidium	1.4×10^3
Giardia	1.3×10^4
E.coli	2.3×10^8

Table. S2-3. PCSWMM model parameters

Parameters	Values
Routing method	Dynamic Wave
Infiltration model	Curve Number
Number of urban drainage catchment	2
Number of conduits	19
Number of junctions	19
Time step resolution of precipitation	5 minutes
Time step computation	60 seconds

The parameter values of the artificial model were initially set based on Derx et al. (2023). To further calibrate the model, we adjusted the storage volume by modifying the parameters of the storage curve in the PCSWMM model. Finally we decided to choose a storage of 28000 m3, the same values suggested by Derx et al. (2023). We conducted four test runs to calculate the Nash–Sutcliffe Efficiency (NSE), which ranged from 0.44 to 0.96, indicating that the model performance varied from satisfactory to excellent in reproducing the observed system behavior.

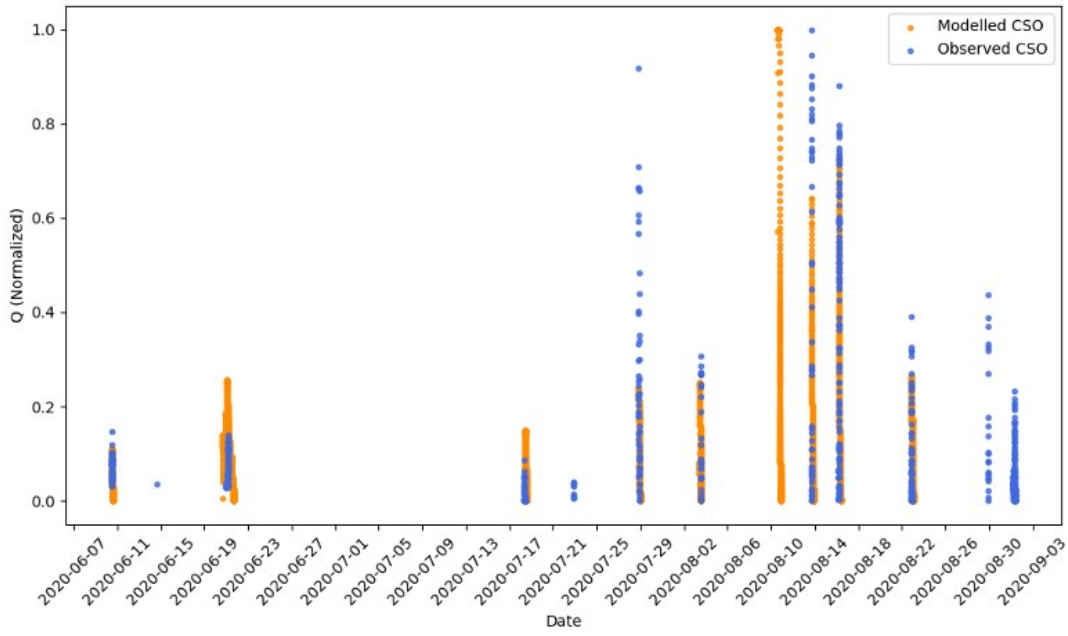

Fig. S2-1. Observed and simulated normalized CSO discharges during rainfall events in June - August 2020

The simulated CSO discharges corresponded with the time and duration of the discharges observed during 8 events in June – August 2020 near the rainfall gauge (Figure S1).

S3 : Bioretention modelling

The design parameters and soil characteristics for bioretention cells used in this study were set based on data from literature and existing case studies (Autixier et al., 2014; Gougeon et al., 2023; Joshi et al., 2020; Rossman & Huber, 2016) as summarized in Fig. 3. The modeling of bioretention relies on data from the literature due to the unavailability of site-specific information. This approach, combined with a case study methodology, allows for the evaluation of the feasibility and performance of the system within a local context while referencing comparable data and is commonly used in the literature (Autixier et al., 2014; Joshi et al., 2020).

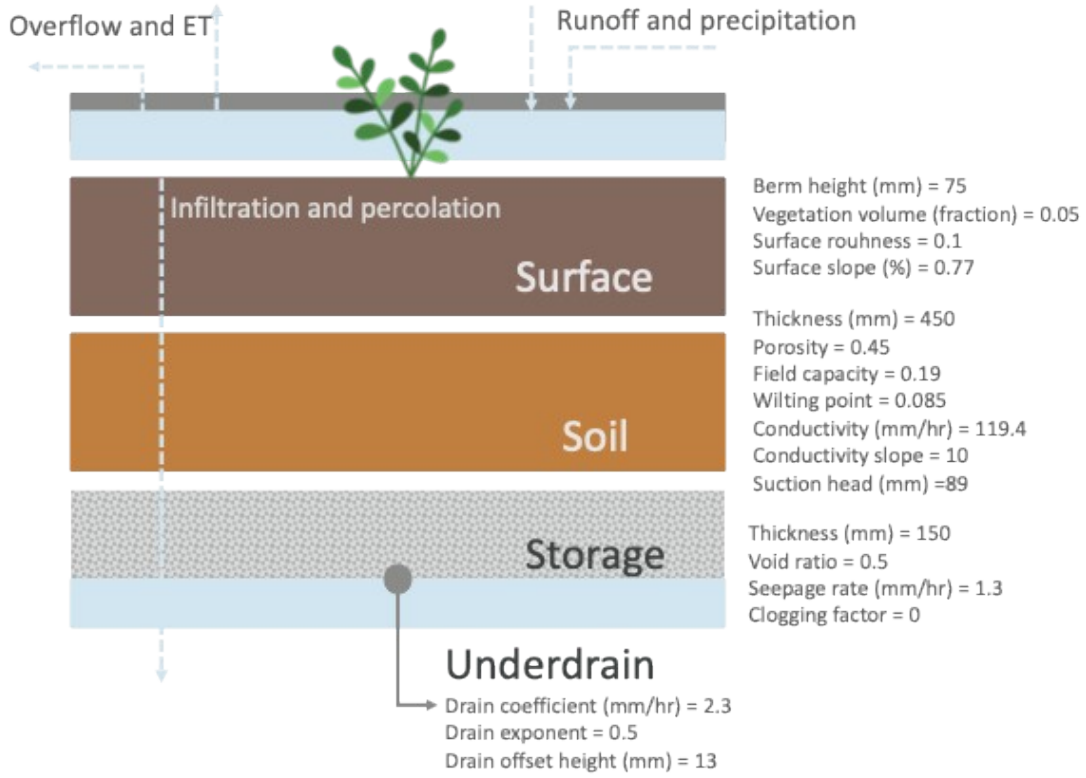

Fig. S3-1. Summary of the parameters' values for each layer of the modeled bioretention cells in PCSWMM

To model bioretention in PCSWMM, some parameters (width & imperviousness) need to be recalculated according to the size of the implemented bioretention (Rossman & Huber, 2016). One of those parameters is the width (W) of the subcatchment, which was calculated as a function of the total area of the sub-catchment and the flow length. Width is a very sensitive parameter (Autixier, 2012), so it is essential to consider it when proposing BGI implementation scenarios. Adding BGI in an existing PCSWMM model (using the built-in LID Editor) creates new flow paths, thus increasing the total flow length (L) in a drainage basin (W=A/L). It is important to note that the width parameter only applies to the part of the sub-catchment not affected by the LID. The width is recalculated for each sub-catchment to more accurately represent the impact of bioretention cell implementation. Assuming a square shape for the added bioretention areas and using the known implementation area (based on the percentage applied), the width parameter can be recalculated accordingly. If the new width calculated with the addition of the LID is greater than the initial width parameter, for example due to the shape of the urban drainage basin, the initial width parameter is retained. The percentage of imperviousness was also recalculated according to the percentage of implemented bioretention (Rossman & Huber, 2016). The modified percentage of imperviousness is the ratio between the remaining impervious area (after adding the bioretention) and the non-bioretention area. Finally, we set initial saturation at 25%, treated impervious areas at 30%, and treated permeable areas at 10%, based on a previous study with similar bioretention setup (Bouattour, 2021).

S4: Water quality data

The background microbial concentration in river water $C_{river,bg \cdot obs}$ in Eq. 1 was characterized using selected statistical distributions suggested by Derx et al. (2023) (Table S4-1). Parameters were fitted

to the observed river data, with Kruskal–Wallis tests guiding distribution selection (p>0.05 p>0.05). Random values were then sampled at each time step and used for each simulation.

Table S4-1 : Observed microbial concentrations in raw wastewater in the Vienna river during basic monitoring from Derx et al. (2023)

Parameter	**Observed dataset** **detected/n**	**Observed mean** **[particles/l]**	**Descriptive statistical parameter** **values gamma distribution: shape/location/scale**	**Kruskal-Wallis p**
Enterococci	21/21	2.1×10^4	0.27/6/1500	0.08
Cryptosporidium	23/26	6.3×10^0	0.6/0.0/0.9	0.95
Giardia	24/26	7.1×10^0	0.3/0.0/1.2	0.09

S5: Rainfall-runoff model (HBV)

The hydrological model follows the vertical structure of the HBV model (Bergström, 1976) with adaptations including an additional groundwater storage, bypass flow, and a modified river routing scheme (Blöschl et al., 2008; Komma et al., 2008). For each raster element, snow, soil moisture, and hillslope processes are simulated hourly. Snow accumulation and melt are represented by a degree-day method, while runoff generation is modeled via three reservoirs for overland flow, interflow, and groundwater flow. Stream routing is implemented using a cascade of linear reservoirs (Szolgay, 2004)

Model calibration and validation used hourly rainfall and air temperature data from nearby meteorological stations for 1990–2018 by Derx et al. (2023). Hydrologic Response Units (HRUs) with similar land use (urban, forest, agricultural) were assigned a priori parameter sets, which were then refined through comparison of simulated and observed hydrographs (Derx et al., 2023). Model performance, assessed using the Nash–Sutcliffe efficiency (NSE), ranged from 0.51 to 0.93 annually, with an overall NSE of 0.77 (Derx et al., 2023).

S6: Additional results - Hydrological model result

63

73

77

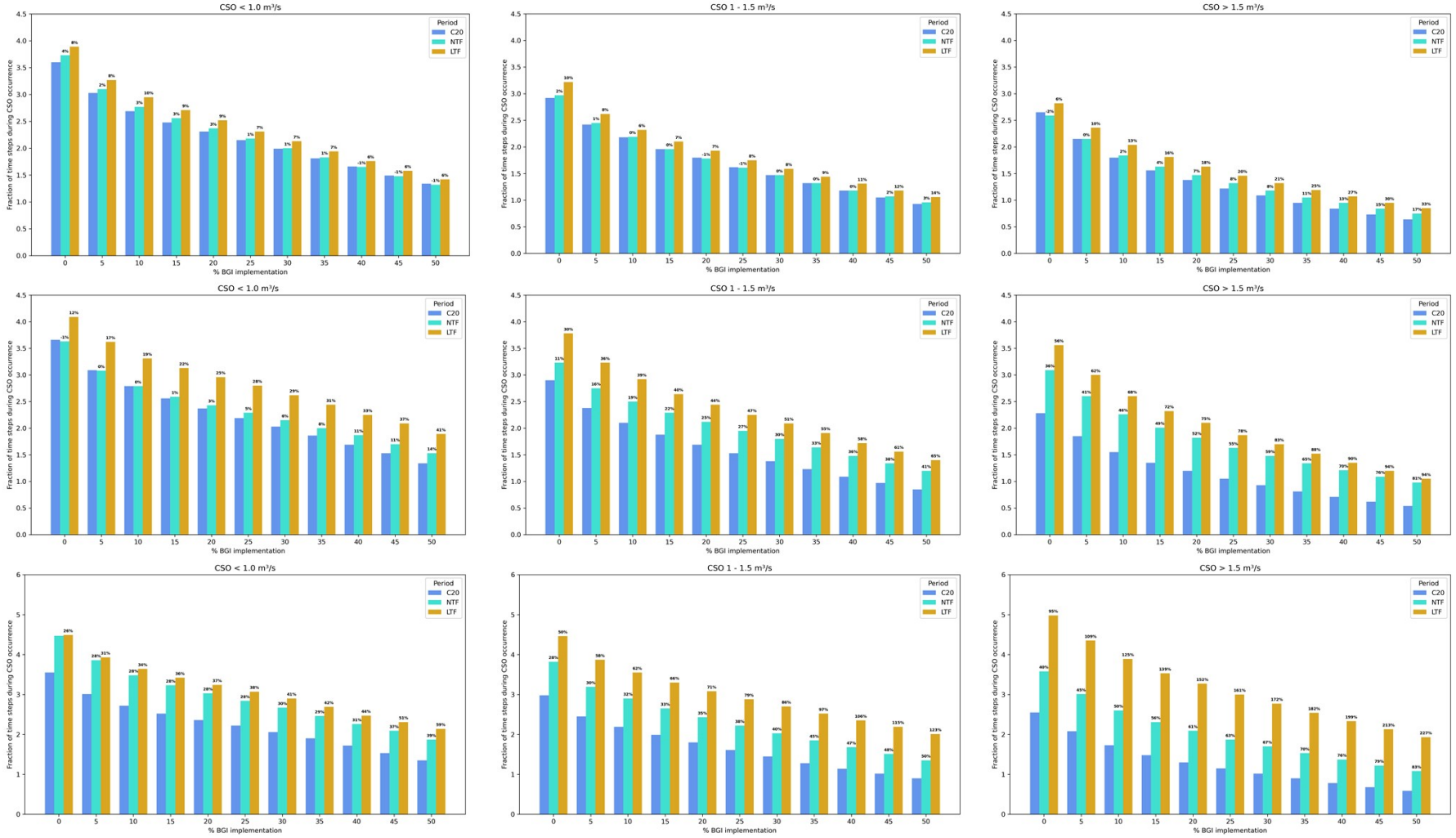

Fig. S6-1. Fraction of 5 min-time steps during CSO occurrence [%] for the C20, NTF and LTF. CSOs are differentiated for <1.0 m3/s, 1 - 1.5 m3/s and >1.5 m3/s. For all the different BGI implementation %. For the three considered climate scenarios

Table. S6-1. Fraction of simulation 5-min time steps with CSOs [%] for the C20, NTF and LTF for different percentages of BGI implementation, the relative change to C20 and the reduction when adding BGI. For climate scenario C73

%BGI	Period	CSO < 1.0 m^3/s (%)	Relative change to C20	Reduction VS no BGI	CSO 1 - 1.5 m^3/s (%)	Relative change to C20	Reduction VS no BGI	CSO > 1.5 m^3/s (%)	Relative change to C20	Reduction VS no BGI
No BGI	C20	3.66	-		2.9	-		2.28	-	
	NTF	3.63	-1%		3.23	11%		3.09	36%	
	LTF	4.09	12%		3.78	30%		3.56	56%	
5%	C20	3.09	-	-16%	2.38	-	-18%	1.85	-	-19%
	NTF	3.08	0%	-15%	2.75	16%	-15%	2.6	41%	-16%
	LTF	3.62	17%	-11%	3.23	36%	-15%	3	62%	-16%
30%	C20	2.03	-	-45%	1.38	-	-52%	0.93	-	-59%
	NTF	2.15	6%	-41%	1.8	30%	-44%	1.48	59%	-52%
	LTF	2.62	29%	-36%	2.09	51%	-45%	1.7	83%	-52%
50%	C20	1.34	-	-63%	0.85	-	-71%	0.54	-	-76%
	NTF	1.53	14%	-58%	1.2	41%	-63%	0.98	81%	-68%
	LTF	1.89	41%	-54%	1.4	65%	-63%	1.05	94%	-71%

Table. S6-2. Fraction of simulation 5-min time steps with CSOs [%] for the C20, NTF and LTF for all percentages of BGI implementation and the additional storage

		63			73			77		
	%BGI	CSO < 1.0 m3/s (%)	CSO 1 - 1.5 m3/s (%)	CSO > 1.5 m3/s (%)	CSO < 1.0 m3/s (%)	CSO 1 - 1.5 m3/s (%)	CSO > 1.5 m3/s (%)	CSO < 1.0 m3/s (%)	CSO 1 - 1.5 m3/s (%)	CSO > 1.5 m3/s (%)
C20	0%	3.6	2.92	2.65	3.66	2.9	2.28	3.55	2.98	2.55
	5%	3.03	2.42	2.15	3.09	2.38	1.85	3.01	2.45	2.08
	10%	2.69	2.18	1.8	2.79	2.1	1.55	2.72	2.19	1.73
	15%	2.48	1.96	1.56	2.56	1.88	1.35	2.52	1.99	1.48
	20%	2.31	1.8	1.38	2.37	1.69	1.2	2.36	1.8	1.3
	25%	2.15	1.62	1.22	2.19	1.53	1.05	2.22	1.61	1.15
	30%	1.99	1.47	1.09	2.03	1.38	0.93	2.06	1.45	1.02
	35%	1.81	1.32	0.95	1.86	1.23	0.81	1.9	1.28	0.9
	40%	1.66	1.18	0.84	1.69	1.09	0.71	1.72	1.14	0.78
	45%	1.49	1.05	0.73	1.53	0.97	0.62	1.53	1.02	0.68
	50%	1.34	0.93	0.64	1.34	0.85	0.54	1.35	0.9	0.59
	storage	3.0	2.58	2.34	2.98	2.55	1.96	2.91	2.65	2.26
NTF	0%	3.73	2.97	2.59	3.63	3.23	3.09	4.47	3.82	3.58
	5%	3.1	2.45	2.15	3.08	2.75	2.6	3.86	3.19	3.01
	10%	2.77	2.19	1.84	2.79	2.5	2.26	3.48	2.9	2.6
	15%	2.56	1.96	1.63	2.59	2.29	2.01	3.23	2.65	2.31
	20%	2.37	1.78	1.47	2.43	2.12	1.82	3.03	2.43	2.09
	25%	2.18	1.61	1.32	2.29	1.95	1.63	2.84	2.22	1.87
	30%	2.0	1.47	1.18	2.15	1.8	1.48	2.67	2.03	1.7
	35%	1.83	1.32	1.05	2.0	1.64	1.34	2.46	1.85	1.53
	40%	1.65	1.18	0.95	1.87	1.48	1.21	2.26	1.68	1.37
	45%	1.48	1.07	0.84	1.7	1.34	1.09	2.09	1.51	1.22
	50%	1.32	0.96	0.75	1.53	1.2	0.98	1.87	1.35	1.08
	storage	3.09	2.63	2.27	3.04	2.94	2.77	3.81	3.45	3.19
LTF	0%	3.89	3.22	2.82	4.09	3.78	3.56	4.49	4.46	4.98

	5%	3.27	2.62	2.36	3.62	3.23	3.0	3.93	3.87	4.35
	10%	2.95	2.32	2.04	3.31	2.92	2.6	3.64	3.55	3.89
	15%	2.71	2.1	1.81	3.13	2.64	2.32	3.42	3.3	3.53
	20%	2.52	1.93	1.63	2.96	2.44	2.1	3.24	3.08	3.27
	25%	2.31	1.75	1.46	2.8	2.25	1.87	3.07	2.88	3.0
	30%	2.13	1.59	1.32	2.62	2.09	1.7	2.9	2.7	2.77
	35%	1.94	1.44	1.19	2.44	1.91	1.52	2.69	2.52	2.54
	40%	1.76	1.31	1.07	2.25	1.72	1.35	2.47	2.35	2.33
	45%	1.58	1.18	0.95	2.09	1.56	1.2	2.31	2.19	2.13
	50%	1.42	1.06	0.85	1.89	1.4	1.05	2.14	2.01	1.93
	storage	3.26	2.84	2.5	3.54	3.45	3.21	3.86	4.12	4.59

S7: Additional results - Microorganisms' concentration in the river

		Enterococci	*Cryptosporidium*	*Giardia*
63	C20	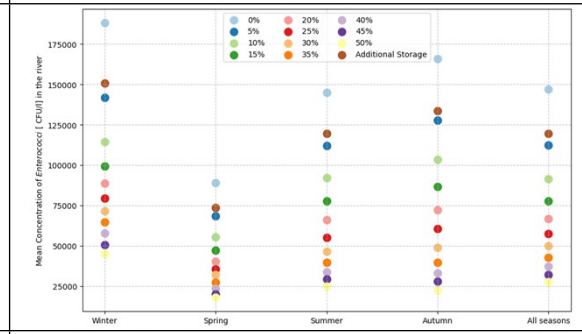	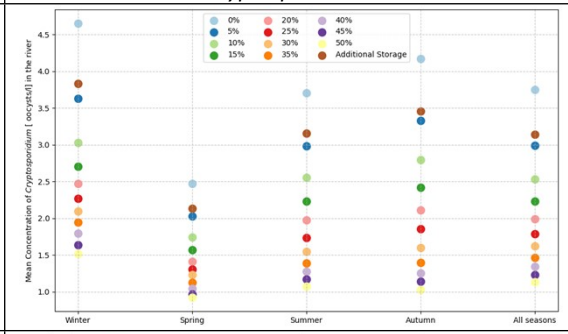	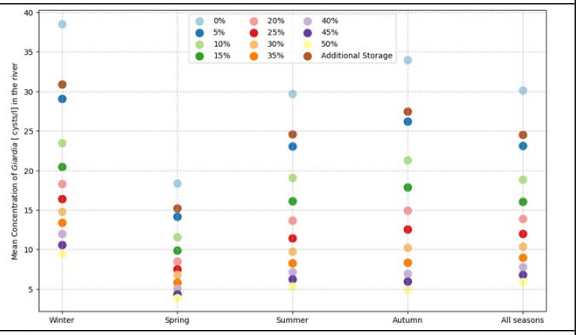
	NTF	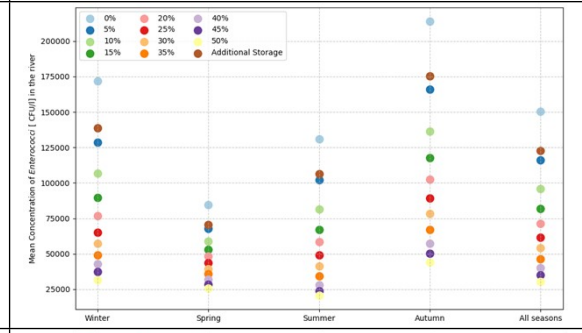	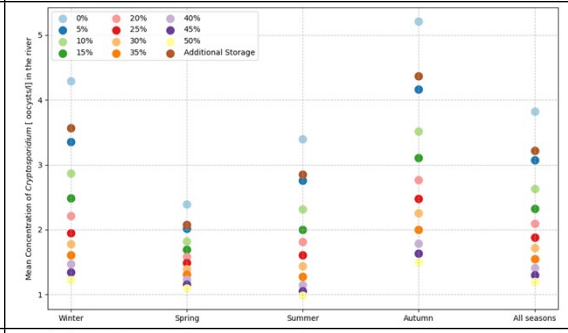	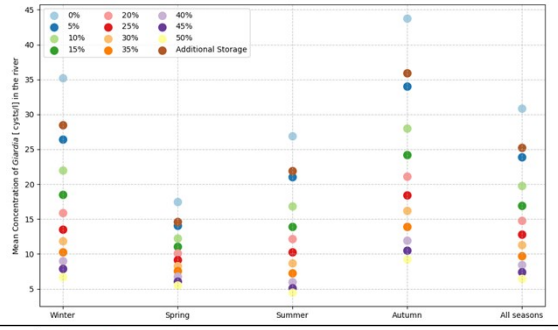
	LTF	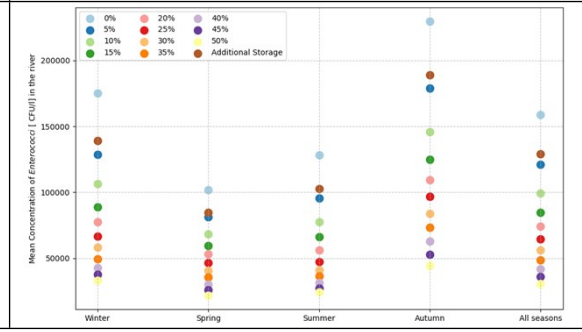	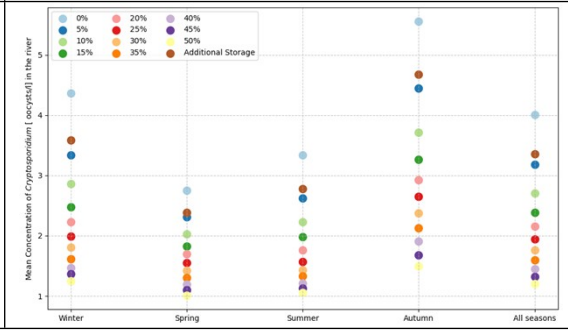	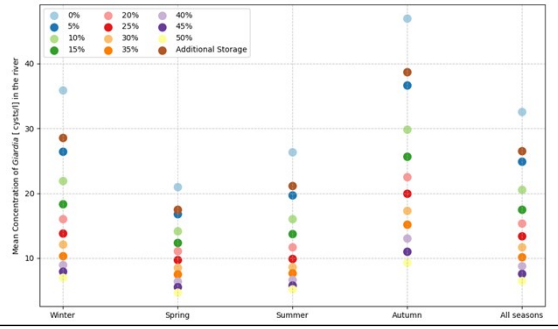

73	C20	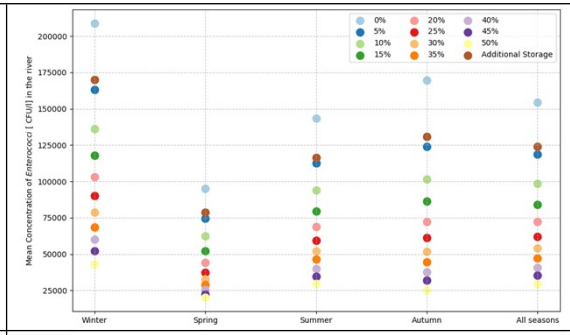	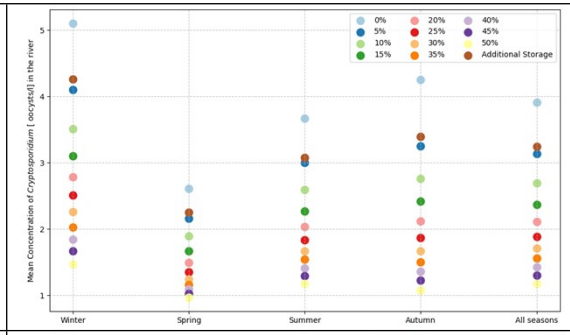	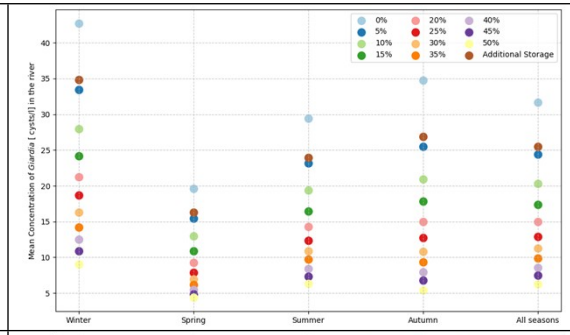
	NTF	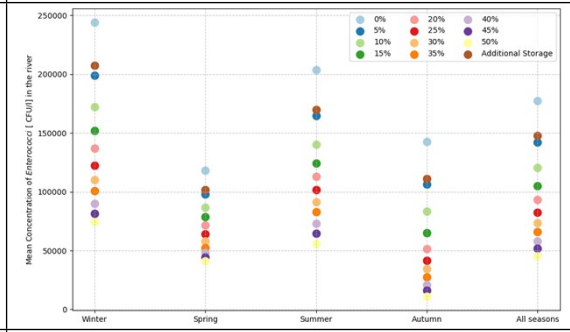	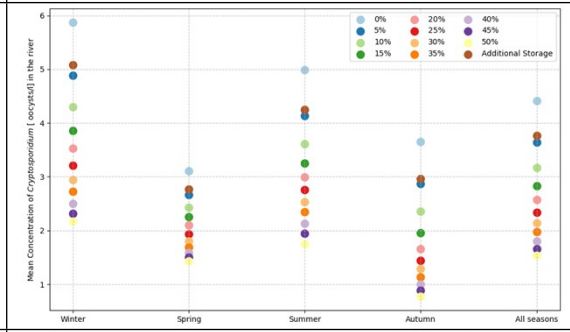	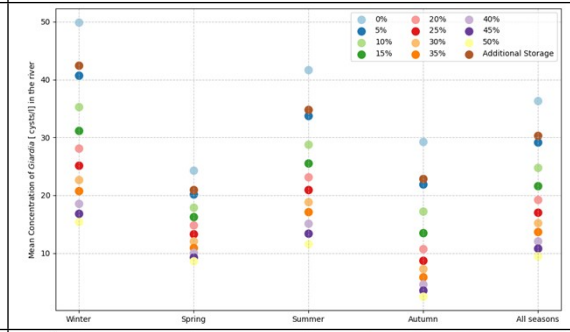
	LTF	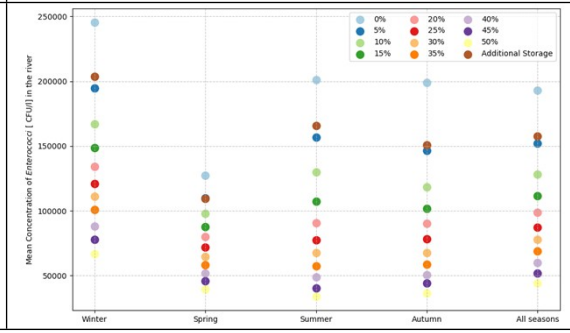	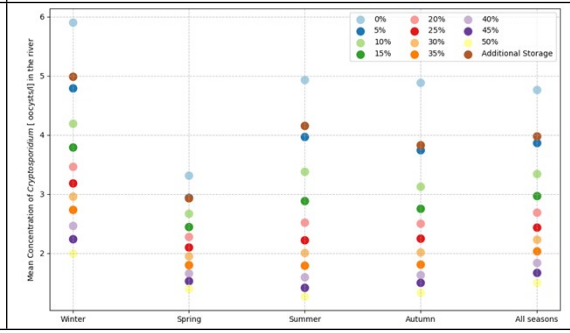	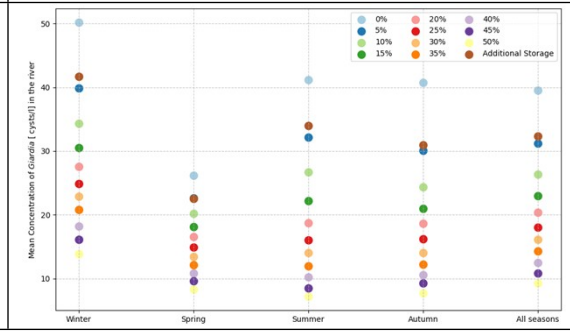

Fig S7-1. Mean concentration of Enterococci [CFU/l], Cryptosporidium [oocysts/l] and Giardia [cysts/l] for the three considered climate scenario per season. The mean concentration in river water is calculated over 30 years of simulation time for C20, NTF and LTF periods

		63	73	77
Cryptosporidium	Winter	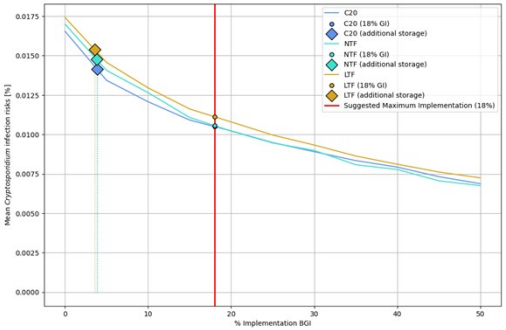 C20 Storage %BGI: 3.88% NTF Storage %BGI: 3.83% LTF Storage %BGI: 3.57%	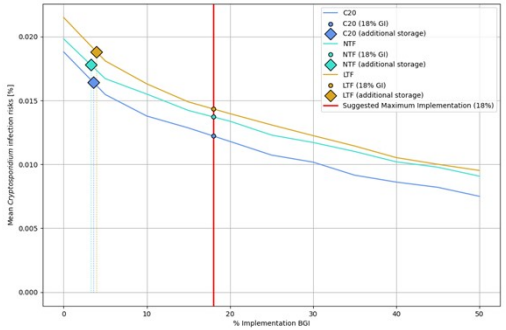 C20 Storage %BGI: 3.56% NTF Storage %BGI: 3.27% LTF Storage %BGI: 3.96%	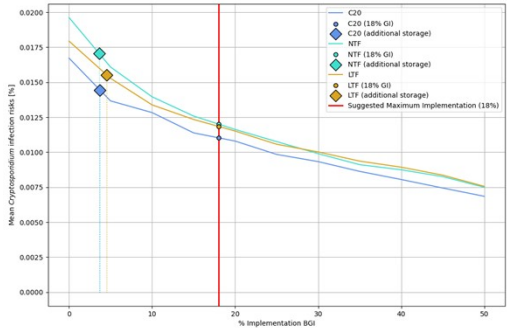 C20 Storage %BGI: 3.73% NTF Storage %BGI: 3.64% LTF Storage %BGI: 4.55%
	Spring	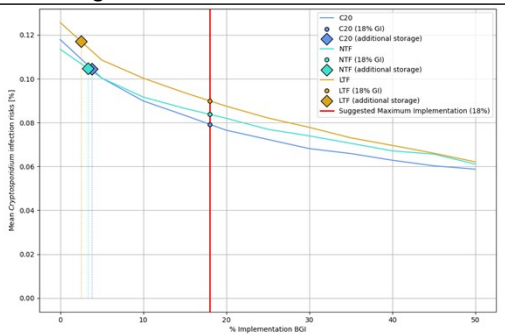 C20 Storage %BGI: 3.82% NTF Storage %BGI: 3.35% LTF Storage %BGI: 2.49%	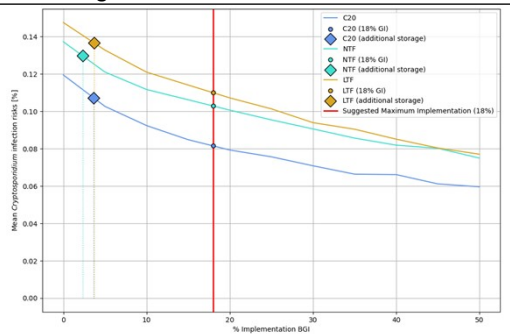 C20 Storage %BGI: 3.66% NTF Storage %BGI: 2.31% LTF Storage %BGI: 3.68%	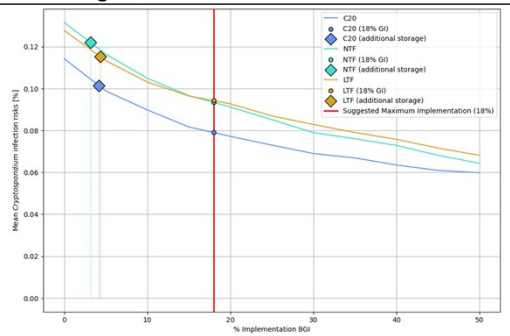 C20 Storage %BGI: 4.18% NTF Storage %BGI: 3.15% LTF Storage %BGI: 4.34%

	Summer	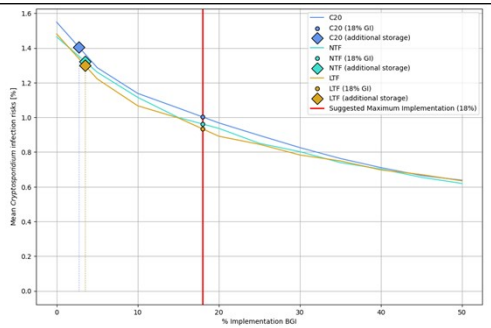 C20 Storage %BGI: 2.75 NTF Storage %BGI: 3.51 LTF Storage %BGI: 3.49	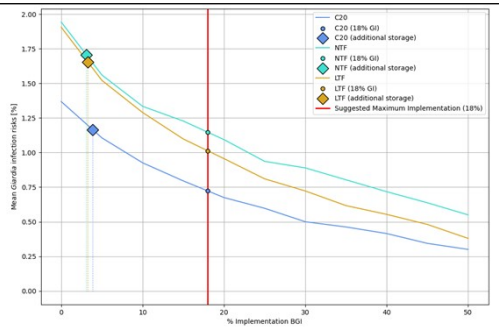 C20 Storage %BGI 3.88% NTF Storage %BGI: 3.08% LTF Storage %BGI: 3.27%	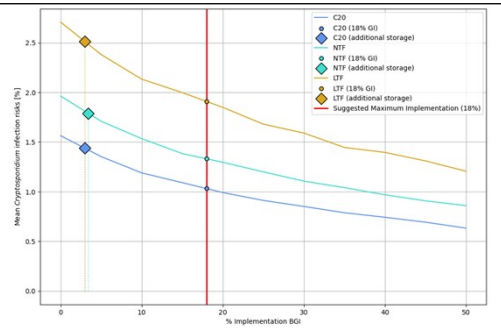 C20 Storage %BGI: 2.99% NTF Storage %BGI: 3.41% LTF Storage %BG:I 2.95%
	Autumn	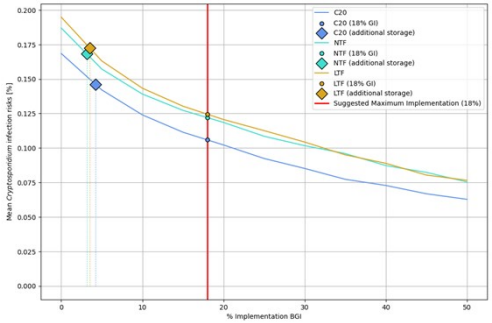 C20 Storage %BGI: 4.26% NTF Storage %BGI: 3.15% LTF Storage %BGI: 3.51%	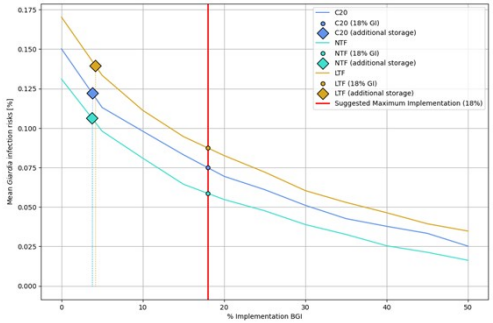 C20 Storage %BGI: 3.77% NTF Storage %BGI: 3.75% LTF Storage %BGI: 4.18%	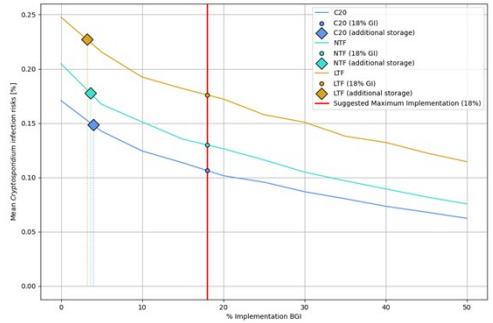 C20 Storage %BGI: 3.96% NTF Storage %BGI: 3.64% LTF Storage %BGI: 3.19%
Gi ar	Winter	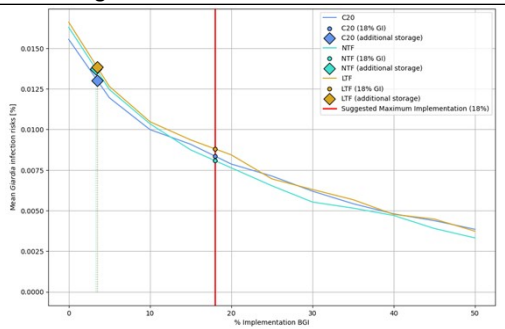 C20 Storage %BGI: 3.51%	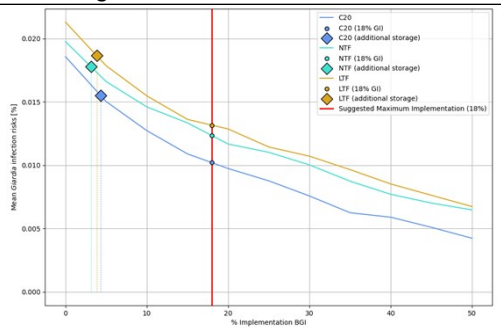 C20 Storage %BGI: 4.34%	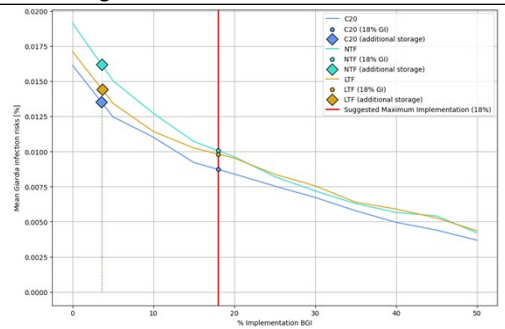 Winter - Giardia - C20 Storage %BG: 3.58

		NTF Storage %BGI: 3.36% LTF Storage %BGI: 3.51%	NTF Storage %BGI: 3.15% LTF Storage %BGI: 3.83%	Winter - Giardia - NTF Storage %BG: 3.61 Winter - Giardia - LTF Storage %BG: 3.69
	Spring	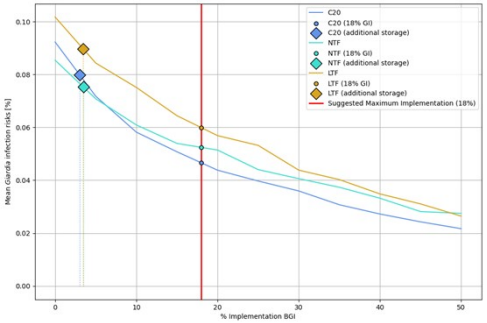 C20 Storage %BGI: 3.01% NTF Storage %BGI: 3.47% LTF Storage %BGI: 3.46%	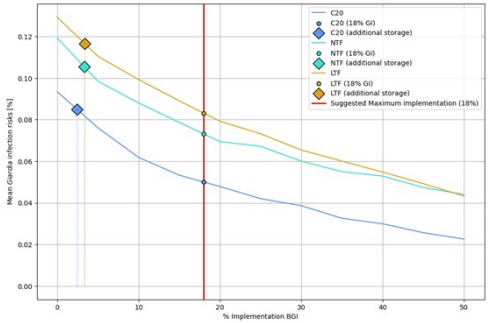 C20 Storage %BGI: 2.43% NTF Storage %BGI: 3.30% LTF Storage %BGI: 3.37%	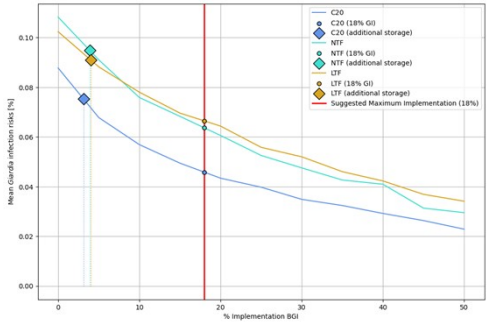 C20 Storage %BGI: 3.14% NTF Storage %BGI: 3.89% LTF Storage %BGI: 4.02%
	Summer	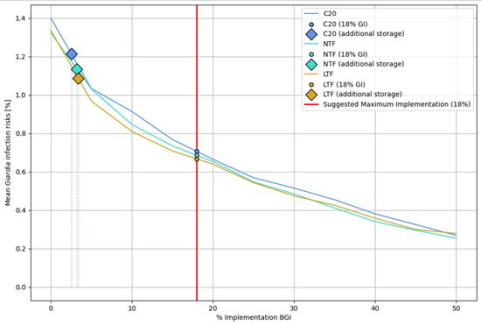 C20 Storage %BGI: 2.54% NTF Storage %BGI: 3.21% LTF Storage %BGI: 3.39%	 C20 Storage %BGI: 3.88% NTF Storage %BGI: 3.08% LTF Storage %BGI: 3.27%	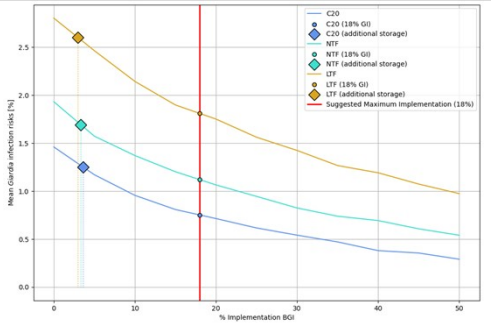 C20 Storage %BGI: 3.61% NTF Storage %BGI: 3.33% LTF Storage %BGI: 2.96%

	Automn	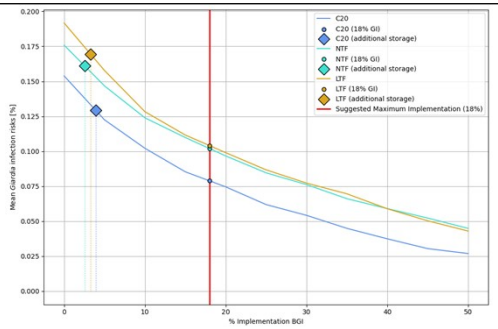 C20 Storage %BGI: 3.93% NTF Storage %BGI: 2.54% LTF Storage %BGI: 3.28%	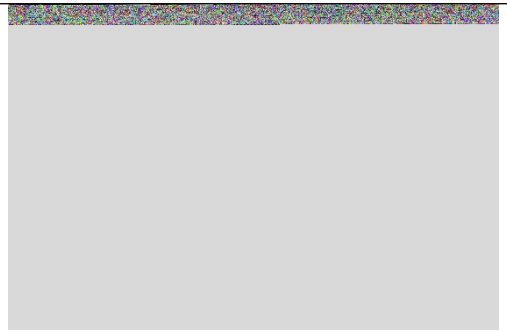 C20 Storage %BGI: 3.77% NTF Storage %BGI: 3.75% LTF Storage %BGI: 4.18%	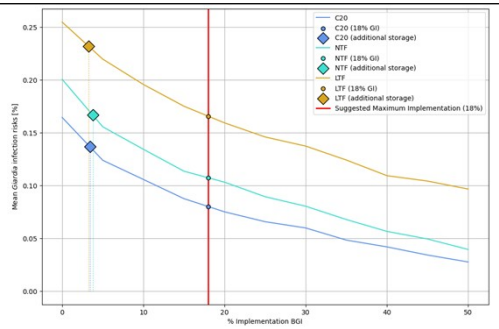 C20 Storage %BGI: 3.43% NTF Storage %BGI: 3.77% LTF Storage %BGI: 3.28%

Fig S7-2. Mean Cryptosporidium and Giardia infection risks [%] per person and exposure event during recreational use of river water calculated over 30 years of simulation time for the C20, NTF and LTF periods as function of BGI implementation (continuous lines). Diamonds represent the probability of infection when additional storage is added, as well as the percentage of green infrastructure required to achieve the same reduction in infection risk. Red line and dots represent the maximum suggested implementation

63	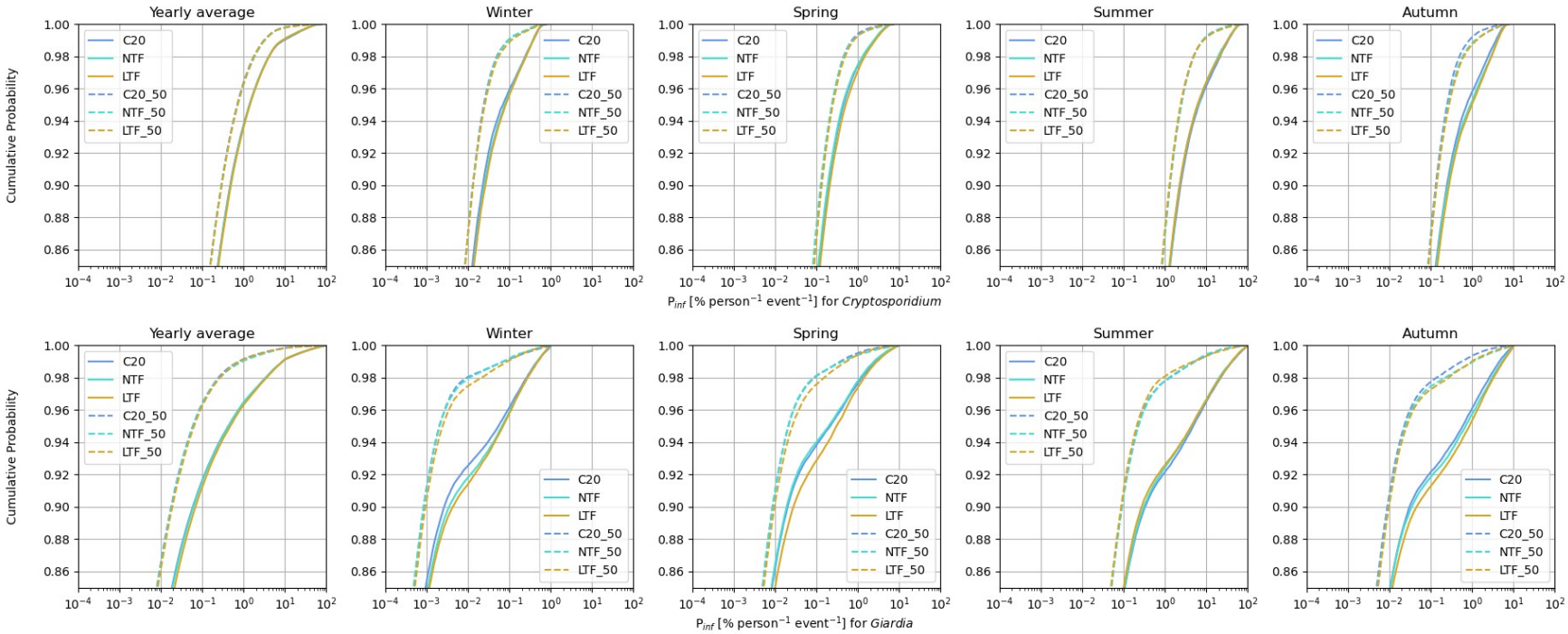 Yearly average Winter Spring Summer Autumn Cumulative Probability C20 NTF LTF C20_50 NTF_50 LTF_50 P_{inf} [% person^{-1} event^{-1}] for *Cryptosporidium* P_{inf} [% person^{-1} event^{-1}] for *Giardia*
73	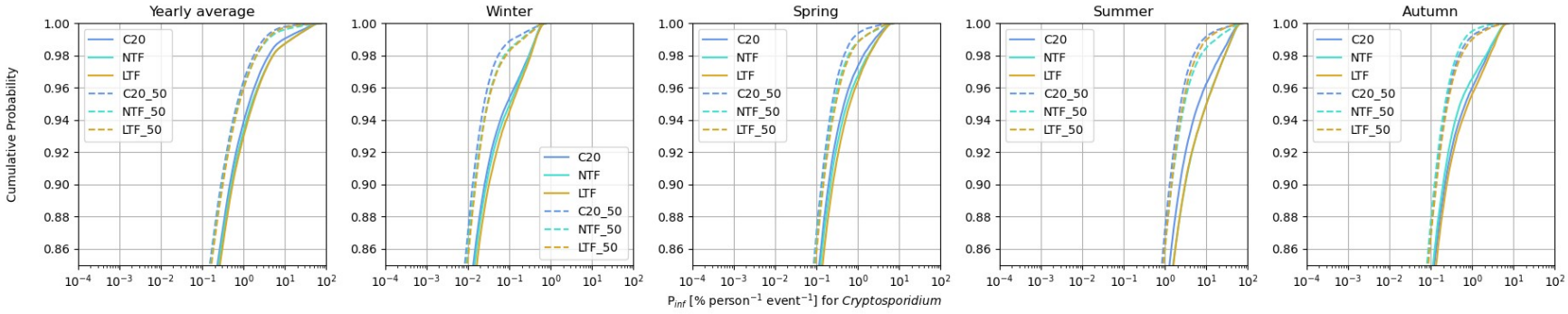 Yearly average Winter Spring Summer Autumn Cumulative Probability C20 NTF LTF C20_50 NTF_50 LTF_50 P_{inf} [% person^{-1} event^{-1}] for *Cryptosporidium*

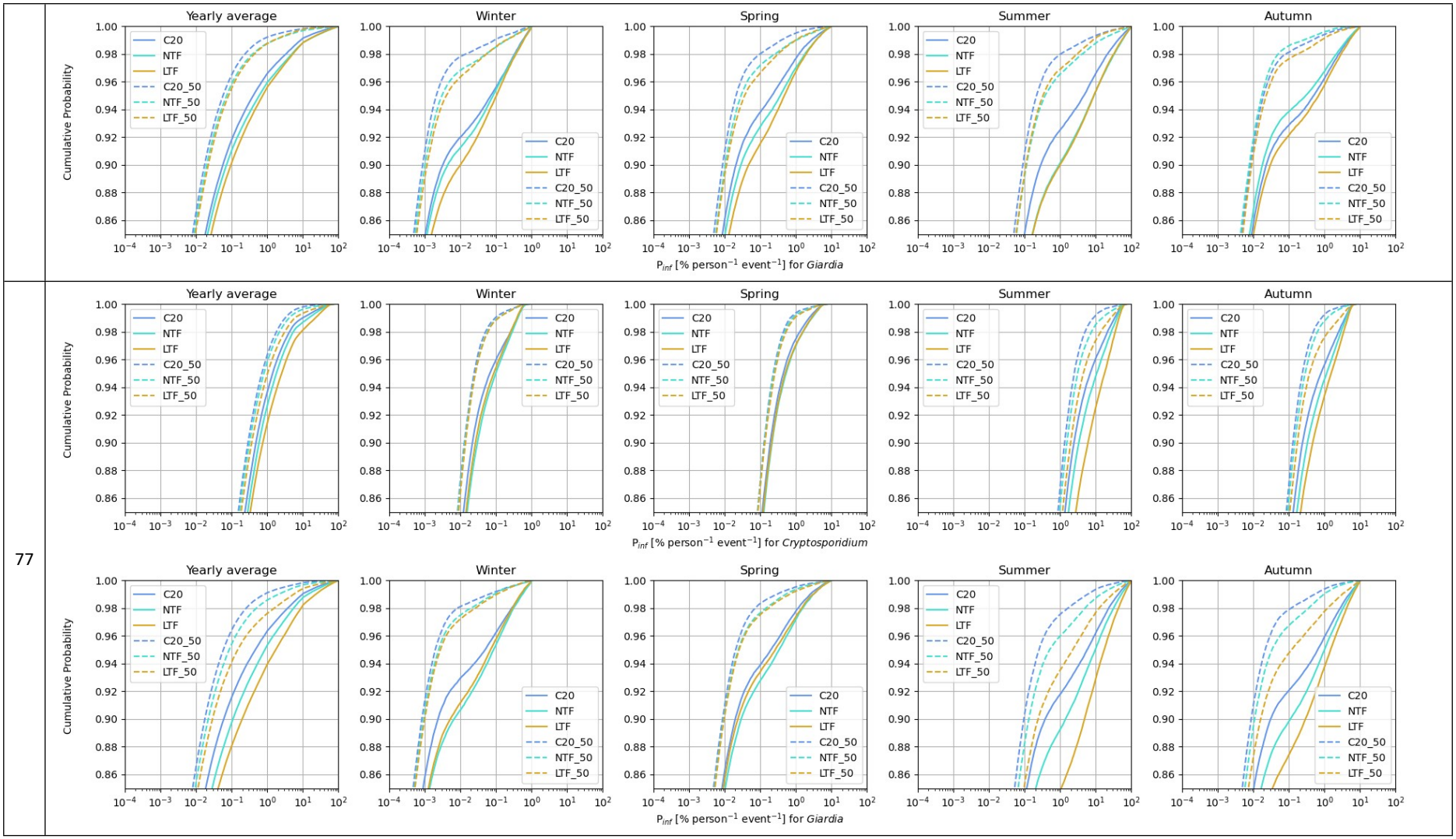

Fig . S7-3. Cumulative probability distributions of the upper percentile infection risks [% per person and exposure event] for Cryptosporidium and Giardia during recreational use in the river downstream of sewage emissions from CSOs over 30 years of simulation time for C20, NTF and LTF for the three considered climate scenario (full lines : no BGI, dotted lines : 50% BGI implementation)

S8: Additional results – Time series

For these results, we decided to show the risk of infection and the CSO flow for one summer for each planning horizon. For each planning horizon, we selected a representative month of July based on the data without BGI. The median is based on the adjusted risk during CSO events, and then we extracted the month of July for this year since it is one of the hottest months and people are more likely to swim during this period. We selected the C73 climate scenarios and *Giardia* to generate those results.

C20 (1995)	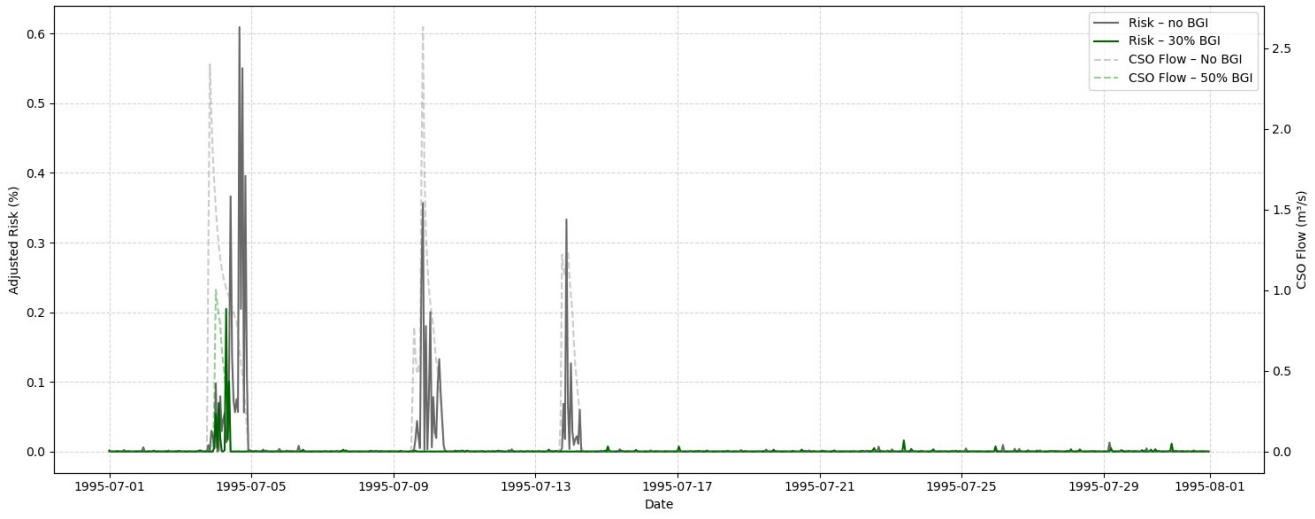
NTF (2049)	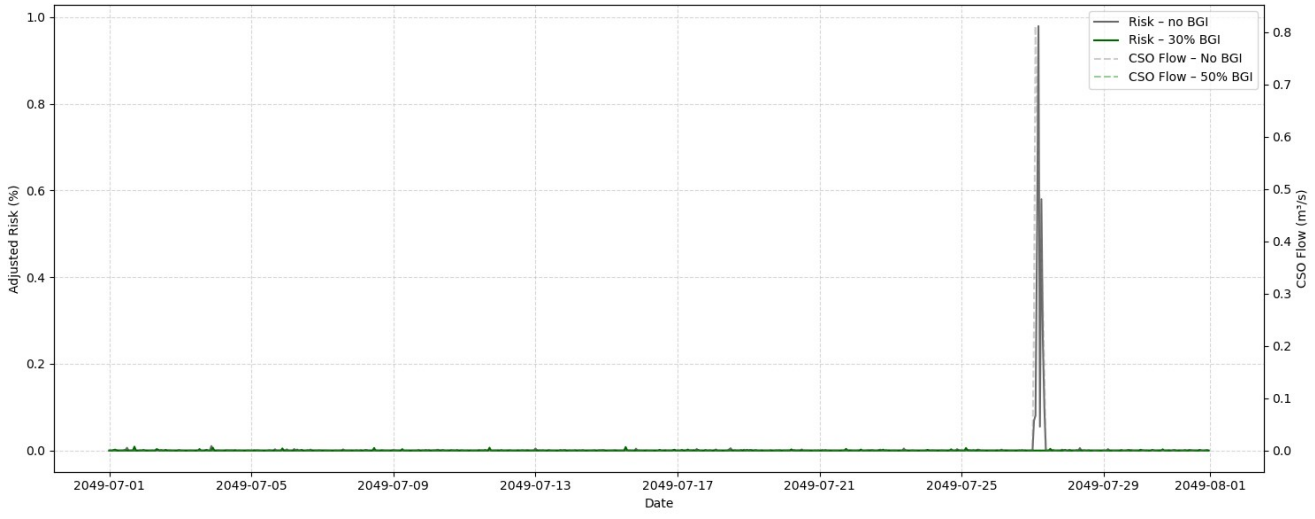

LTF (2075)	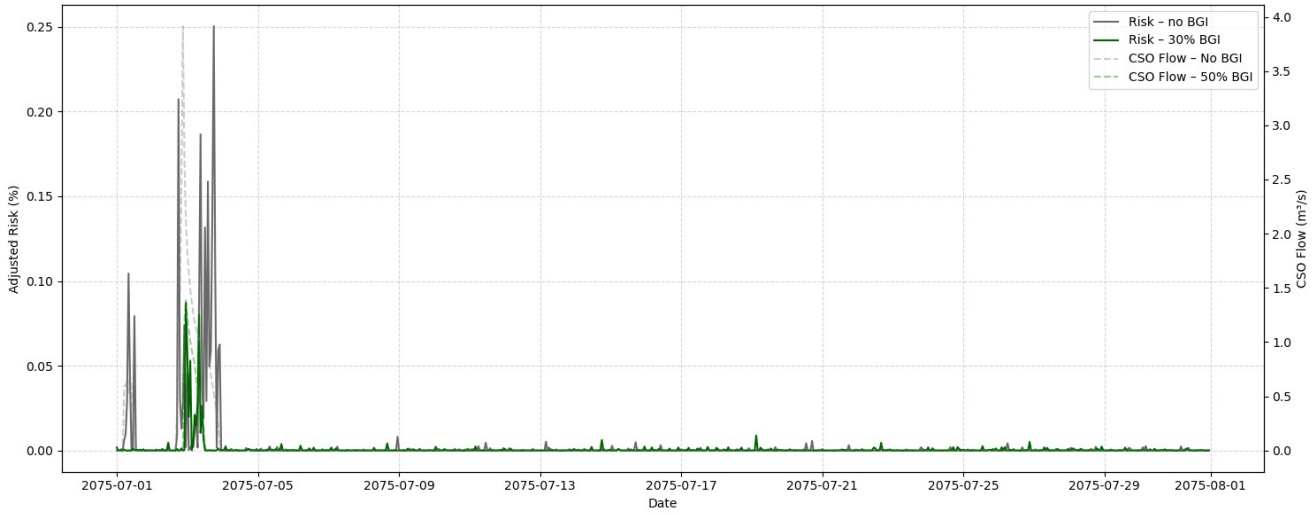

Fige S8-1. Risk of infection for Giardia for a representative month of July for each planning horizon for the climate scenario C73.

Figure S8-1 shows that the risk of infection and the CSO flow reducing with the implementation of BGI. We can also observe that the increase in infection risk does not happen immediately after a CSO event. There is a brief delay between the CSO event and the increase of risk suggesting the risk can remain high even when after the CSO event has ended.

S9: Sensitivity analysis

We performed a linear sensitivity analysis on both the background pathogen concentration in the river (C0) and the concentration caused by CSO events. By varying each factor proportionally around its baseline ($\pm$ 50%), and the resulting change in infection risk was evaluated for both *Giardia* and *Cryptosporidium*.

For *Giardia*, the sensitivity to the background concentration in the river (C0) remains consistently low across all BGI implementation levels and planning horizons, with values close to zero. indicating that variations in river background concentrations have minimal influence on the infection risk. In contrast, the sensitivity to CSO-related concentrations is higher (≈0.7, approaching 1), which shows that the infection risk responds almost proportionally to changes in CSO concentration. This means that CSO discharges are the dominant driver of *Giardia*-related health risk.

For *Cryptosporidium* the risk sensitivity varies depending on the percentage of BGI implemented. The sensitivity to background concentration increases with the percentage of BGI implementation, rising from about 0.2 to 0.6. Conversely, the sensitivity to CSO concentrations is high when little or no BGI is implemented, but decreases as BGI coverage increases, eventually approaching values closer to zero. This suggest that as the system becomes less CSO-driven due to BGI mitigation, background concentrations gradually become the main source of risk.

Therefore, the dominant source of infection risk differs between pathogens. For *Giardia*, CSO discharges is the primary driver of risk regardless of BGI percentage of implementation, since CSO concentrations (concentration from the sewer in the SWMM modeling) are higher than background river levels, making changes in the background concentration less important for the risk of infection.

In contrast, the dominant risk source for *Cryptosporidium* varies with BGI implementation. When BGI coverage is low, CSO discharges have a greater influence on the infection risk, but as BGI reduces CSO flows, background river concentrations increasingly contribute to the overall risk. This reflects the lower *Cryptosporidium* concentrations in CSOs compared to *Giardia*, allowing the influence of background concentrations to grow as mitigation measures are implemented.

$$Sensitivity = \frac{Risk_{+50\%} - Risk_{-50\%} / Risk_{base}}{(1.5 - 0.5)} \qquad \text{Eq 7-1}$$

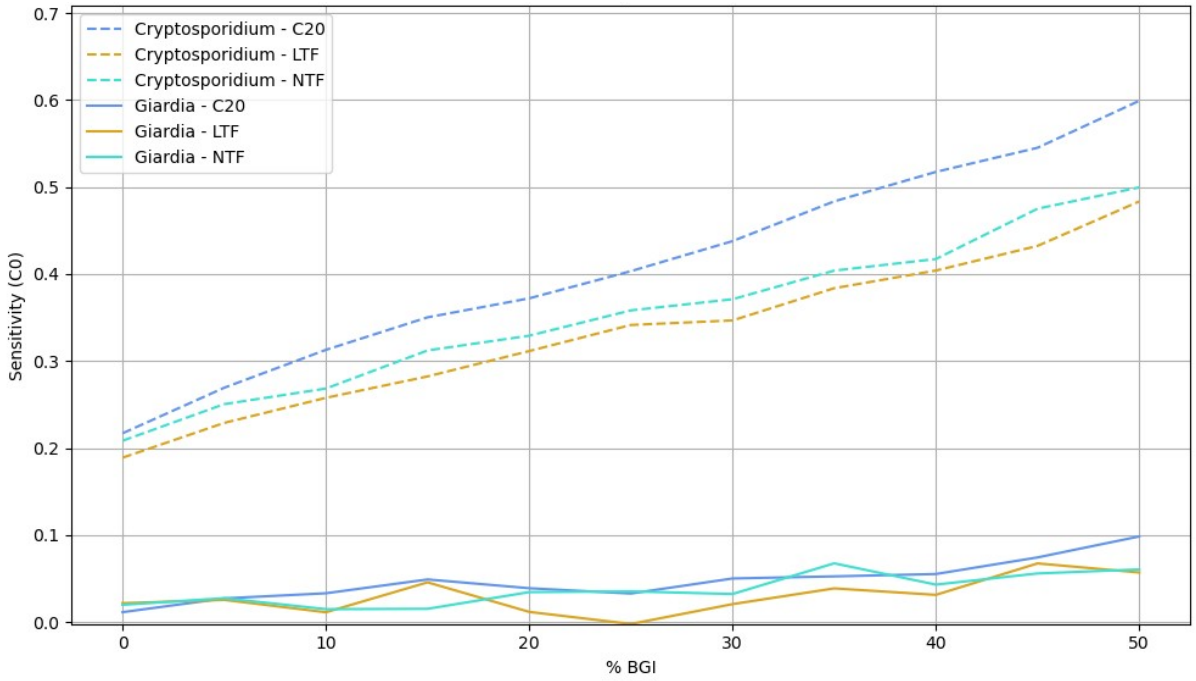

FigS9-1. Risk sensitivity to the background concentration in the river (C0) for Cryptosporidium and Giardia during recreational use in the river downstream of sewage emissions from CSOs over 30 years of simulation time for C20, NTF and LTF for climate scenario C73 (full lines : Giardia, dotted lines : Cryptosporidium)

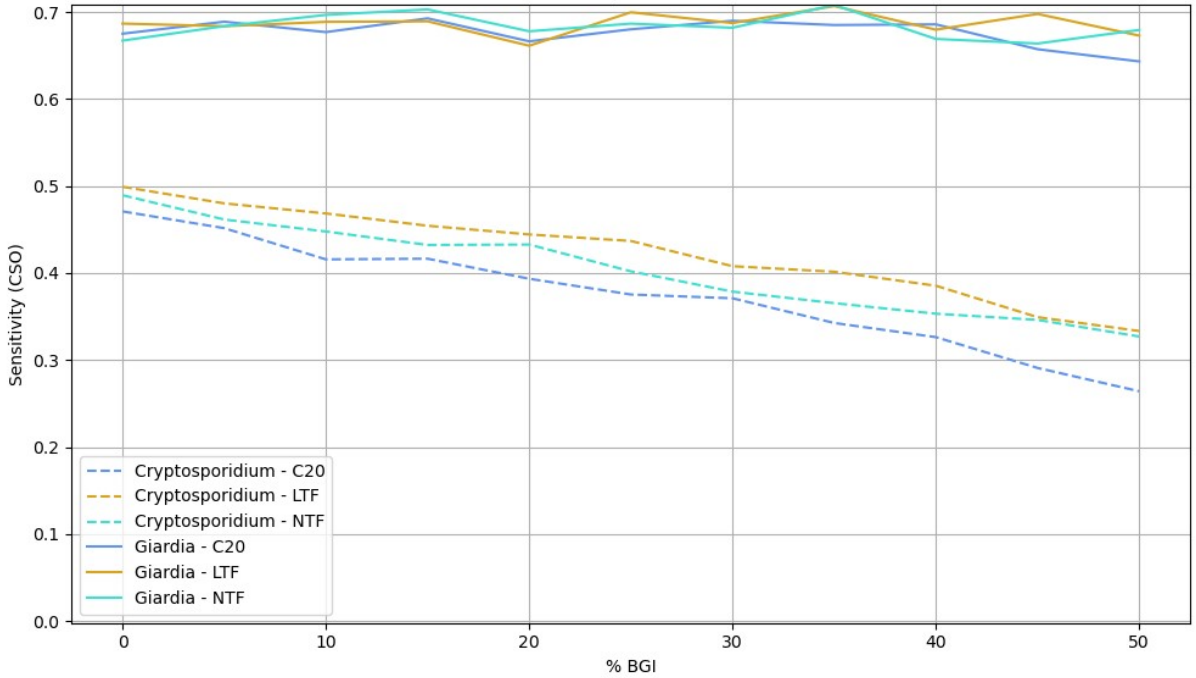

Fig S9-1 . Risk sensitivity to CSO concentration for Cryptosporidium and Giardia during recreational use in the river downstream of sewage emissions from CSOs over 30 years of simulation time for C20, NTF and LTF for climate scenario C73 (full lines : Giardia, dotted lines : Cryptosporidium)

References

Autixier, L. (2012). *GESTION DES EAUX PLUVIALES ET MISE EN PLACE DE CELLULES DE BIO-RÉTENTION : ÉTUDE DE CAS POUR UN SECTEUR URBAIN DU QUÉBEC* Polytechnique Montréal]. Montréal. https://publications.polymtl.ca/984/1/2012_LaureneAutixier.pdf

Autixier, L., Mailhot, A., Bolduc, S., Madoux-Humery, A.-S., Galarneau, M., Prévost, M., & Dorner, S. (2014). Evaluating rain gardens as a method to reduce the impact of sewer overflows in sources of drinking water. *Science of the Total Environment*, *499*, 238-247. https://doi.org/10.1016/j.scitotenv.2014.08.030

Bergström, S. (1976). *Development and application of a conceptual runoff model for Scandinavian catchments*.

Blöschl, G., Reszler, C., & Komma, J. (2008). A spatially distributed flash flood forecasting model. *Environmental Modelling & Software*, *23*(4), 464-478. https://doi.org/10.1016/j.envsoft.2007.06.010

Bouattour, O. (2021). *Caractérisation de l'impact de cellules de biorétention sur la qualité et la quantité des eaux pluviales à Trois-Rivières, Québec* Polytechnique Montréal]. PolyPublie. https://publications.polymtl.ca/9184/

Derx, J., Müller-Thomy, H., Kılıç, H. S., Cervero-Arago, S., Linke, R., Lindner, G., Walochnik, J., Sommer, R., Komma, J., Farnleitner, A. H., & Blaschke, A. P. (2023). A probabilistic-deterministic approach for assessing climate change effects on infection risks downstream of sewage emissions from CSOs. *Water Research*, *247*, 120746. https://doi.org/10.1016/j.watres.2023.120746

Gougeon, G., Bouattour, O., Formankova, E., St-Laurent, J., Doucet, S., Dorner, S., Lacroix, S., Kuller, M., Dagenais, D., & Bichai, F. (2023). Impact of bioretention cells in cities with a cold climate: modeling snow management based on a case study. *Blue-Green Systems*, *5*(1), 1-17. https://doi.org/10.2166/bgs.2023.032

Joshi, P., Paulo Leitão, J., Maurera, M., & Marcus Bach, P. (2020). Not all SuDS are created equal: Impact of different approaches on combined sewer overflows. *Water Research*, *191*, 116780.

Komma, J., Blöschl, G., & Reszler, C. (2008). Soil moisture updating by Ensemble Kalman Filtering in real-time flood forecasting. *Journal of Hydrology*, *357*(3), 228-242. https://doi.org/https://doi.org/10.1016/j.jhydrol.2008.05.020

Rossman, L. A., & Huber, W. C. (2016). *Storm Water Management Model Reference Manual Volume III – Water Quality*. https://nepis.epa.gov/Exe/ZyPDF.cgi/P100P2NY.PDF?Dockey=P100P2NY.PDF

Szolgay, J. (2004). Multilinear flood routing using variable travel-time discharge relationships on the Hron River. *J. Hydrol. Hydromech*, *52*(4), 303-316.